Discover Oncology

Research

Identification of PD-L1-related biomarkers for selecting gastric adenocarcinoma patients for PD-1/PD-L1 inhibitor therapy

Bo-Ya Li[1] · Hui-Ling Li[1] · Fei-Er Zeng[2] · Xuan-Yu Luan[3] · Bi-Qing Liu[4] · Zhi-Zhou Wang[1] · Lan Zhang[1] · Xian-Zhe Dong[1]

Received: 11 November 2024 / Accepted: 25 April 2025
Published online: 08 May 2025

Abstract

PD-1/PD-L1 inhibitors have been used to treat gastric cancer, and PD-L1 expression has been identified as a biomarker for predicting the effectiveness of immunotherapy in the treatment of gastric cancer. However, PD-L1 expression prediction for immunotherapy response is inaccurate, and improved response biomarkers are required. Thus, it is important to identify additional biomarkers that can predict the responses to PD-1/PD-L1 monoclonal antibodies in gastric cancer. In this study, GO and KEGG enrichment analysis of 142 DEGs co-expressed with PD-L1 were performed, and 41 genes were identified based on the intersection of the mRNA-significant GO term network and the mRNA-significant signalling pathway network. Further intersection analysis of the 41 candidate genes and 137 positive immunotherapy response genes indicated that BATF2 significantly affects the overall survival of GC patients. The transcription factor prediction for BATF2 identified additional potential predictors and therapeutic targets for GC. STAT and IRF family members were predicted to be transcription factors for BATF2. In addition, BATF2 knockdown significantly promoted GC cell growth, and PD-L1 expression was upregulated in si-BATF2-treated MKN-45 cells. Thus, BATF2 may serve as a biomarker for predicting the efficacy of PD-L1 blockade therapy in GC. BATF2 acts as a tumour suppressor gene during the development of GC. BATF2 is closely related to PD-L1 expression in GC, and high BATF2 expression positively correlates with low PD-L1 expression. BATF2 can be used as a potential biomarker and therapeutic target for responding to anti-PD-1 and anti-PD-L1 immunotherapies in GC.

Keywords Gastric adenocarcinoma · PD-L1 co-expression genes · Prospective biomarkers · Adjuvant therapeutic targets · BATF2

Abbreviations

ANOVA	Analysis of variance
BATF2	Basic leucine zipper ATF-like transcription factor 2
BP	Biological process

Bo-Ya Li and Hui-Ling Li have contributed equally to this work and shared the first authorship.

Supplementary Information The online version contains supplementary material available at https://doi.org/10.1007/s12672-025-02515-1.

✉ Lan Zhang, lanizhg@126.com; ✉ Xian-Zhe Dong, dongxianzhe@163.com | [1]Department of Pharmacy, Xuanwu Hospital, Capital Medical University, National Clinical Research Centre for Geriatric Diseases, Beijing, China. [2]Department of Genetics and Genome Biology, Leicester Cancer Research Centre, University of Leicester, Leicester LE2 7LX, UK. [3]School of Chinese Materia Medica, Tianjin University of Traditional Chinese Medicine, Tianjin, China. [4]Department of Pharmacy, Children's Hospital Affiliated to Capital Institute of Paediatrics, Beijing, China.

CAG	Chronic atrophic gastritis
CC	Cellular components
cDNA	Complementary DNA
CPS	Combined positive score
DEGs	Differentially expressed genes
DMEM	Dulbecco's Modified Eagle Medium
ELISA	Enzyme-linked immunosorbent assay
ES	Enrichment score
FBS	Fetal bovine serum
GSEA	Gene Set Enrichment Analysis
GC	Gastric cancer
GO	Gene Ontology
IM	Intestinal metaplasia
KEGG	Kyoto Encyclopedia of Gene and Genomes
MDSCs	Myeloid-derived suppressor cells
MF	Molecular function
MSI	Microsatellite instability
NAG	Non-atrophic gastritis
NB	Negative binomial
ORR	Objective response rate
PD-1	Programmed cell death protein 1
PD-L1	Programmed cell death ligand 1
PPI	Protein–protein interaction
PWMs	Position weight matrices
SD	Standard deviation
TCGA	The Cancer Genome Atlas
TIGER	Tumour Immunotherapy Gene Expression Resource
TFs	Transcription factors
TFBs	Transcription factor binding sites
TMB	Tumour mutational burden
TPS	Tumour proportion score
VEGF	Vascular endothelial growth factor

1 Introduction

Gastric cancer (GC) is one of the most common malignancies worldwide, and its traditional treatments include surgery, chemotherapy, and radiotherapy. However, the effectiveness of these treatments is limited for advanced or metastatic GC patients [1–3]. In recent years, the emergence of immune checkpoint inhibitors (such as PD-1/PD-L1 inhibitors) has introduced promising new strategies for the treatment of GC. Immune checkpoint inhibitors offer a new treatment option for advanced GC patients, with the advantages of prolonged survival, durable treatment response, and relatively low toxicity [4, 5].

In the clinical application of immunotherapy, especially treatment with PD-1/PD-L1 inhibitors, reliable biomarkers for predicting the treatment response of patients are lacking [6, 7]. PD-L1—a protein on the surface of tumour cells—is used as a biomarker in immunotherapy to predict a patient's response to immune checkpoint inhibitor therapy [8]. Measuring PD-L1 expression enables doctors to identify which GC patients are more likely to benefit from this therapy [9, 10]. However, PD-L1 is not an accurate predictor marker. While high levels of PD-L1 expression are associated with better immunotherapy responses, many patients with low or even negative PD-L1 expression can still benefit from immunotherapy [11, 12]. PD-L1 expression in tumour samples is heterogeneous, i.e., it may vary between regions of the same tumour. This heterogeneity can lead to inconsistent results in detecting PD-L1 biomarker expression, potentially impacting the response prediction in the immunotherapy [13]. Although PD-L1 is a valuable predictor of response to immunotherapy in GC, its limitations indicate that it is not an ideal biomarker [14]. To improve the accuracy of the predictions, it is necessary to combine other biomarkers for a more comprehensive assessment. Integrating other biomarkers

can improve the accuracy and reliability of PD-L1 in predicting response to immunotherapy. A single biomarker often does not fully reflect the immune status of the tumour and the patient's response to treatment; thus, a combination of multiple biomarkers can better assess the patient's response to immunotherapy [15, 16]. Consequently, this study aimed to identify potentially reliable biomarkers in combination with PD-L1 to improve the selection of patients for PD1/PD-L1 inhibitor therapy, optimise treatment plans, and prolong the overall survival of patients.

2 Materials and methods

2.1 Patients and samples

The Cancer Genome Atlas (TCGA) database retrieved mRNA sequencing data and 375 clinical gastric adenocarcinoma samples from 32 surrounding healthy tissues (https://www.cancer.gov/tcga). Patients with additional malignancies were excluded. In this study, the data processing protocols adhered to the TCGA guidelines, including human subject protection and data access policies, as all the data were derived from human subjects. To analyse genetic alterations in GC patients treated with anti-PD1 immunotherapy, cancer studies were assessed using the PRJEB25780 Dataset (Dataset ID: STAD-PRJEB25780_ANTI-PD1). The distribution and proportion of candidate gene basic leucine zipper ATF-like transcription factor 2 (BATF2) in different cell types of clinical samples was determined by conducting the experiment'Dissecting the Single-Cell Transcriptome Network Underlying Gastric Premalignant Lesions and Early Gastric Cancer' (available in the Tumour Immunotherapy Gene Expression Resource; http://tiger.canceromics.org/#/singleCellImmune).

2.2 Differential expression analysis

Differential expression analysis utilises normalised read count data and statistical analysis to identify quantifiable differences in expression levels between the experimental groups. DESeq2, based on a negative binomial (NB) distribution, was used to identify differentially expressed genes between the test and reference groups for each pairwise contrast. The Wald test is a default hypothesis test applied to the parameters estimated using the maximum likelihood in DESeq2. Therefore, differential expression analysis was conducted by comparing mRNA expression in human stomach cancerous tissues and neighbouring normal tissues using DESeq2 R software and Wald significance tests. Differential expression analysis in DESeq2 uses a generalised linear model of the form:

$$K_{ij} \sim NB\left(\mu_{ij}, \alpha_i\right),$$
$$\mu_{ij} = s_{ij} q_{ij},$$
$$\log_2\left(q_{ij}\right) = x_j \beta_i$$

The Kij raw count for gene i and sample j was modelled using an NB distribution with fitted mean μij and gene-specific dispersion parameter αi. The fitted mean was considered 'normalised counts' scaled by a normalisation factor and is composed of a sample-specific size factor sij and a parameter qij proportionate to the sample j's estimated true fragment concentration. The coefficients i represent the log2 for gene i within each column of the model matrix x. Notably, the model may be expanded to employ sample- and gene-dependent normalisation factors sij, and p values less than 0.05 were regarded as statistically significant.

2.3 PD-L1-mRNAs co-expression network analysis

A co-expression network determines whether a gene exhibits a coordinated expression pattern across a sample collection. This co-expression network can be expressed as a gene–gene similarity matrix, which may be used for subsequent analyses. Therefore, a co-expression analysis was performed to investigate the association between PD-L1 and TCGA genes in GC. A network of mRNAs-PD-L1 co-expression was constructed using the core function of the R package. Based on Pearson correlation coefficients and p-values, pairings of significant correlations were selected while developing the network. Statistical significance was set at $p < 0.05$.

The prediction of protein–protein interaction (PPI) combines bioinformatics and structural biology to annotate cellular locations and biological functions of proteins. A PPI network was reconstructed and obtained from the STRING database

(accessed https://cn.string-db.org/, Version 11.5, 01/06/2022) [17]. We used the minimum required interaction score for high confidence (0.7) [18]. PPIs with a combined score of > 0.7 were considered significant for determining the association between genes and node degrees.

2.4 Gene Ontology (GO), Kyoto Encyclopaedia of Gene and Genomes (KEGG) pathway and Gene Set Enrichment Analysis (GSEA) enrichment

GO and KEGG analyses are the most common functional analysis tools. Statistical and enrichment analyses of GO and KEGG functional profiles of genes and clusters of genes were performed using the Cluster Profiler package in R. We used the hypergeometric distribution test to assess whether these genes were significantly enriched in a particular biological process or pathway. By calculating the *p*-value of the hypergeometric distribution, we can determine how likely it is that the observed enrichment occurred by chance. If the *p*-value is small, it is difficult to observe such enrichment in a random situation. Therefore, we can assume that this functional category or pathway is significantly enriched in our list of genes. The user data mapping module of the KEGG database (accessed at https://www.genome.jp/kegg/, 01/06/2022) was used to visualise the highly enriched pathways.

$$p = 1 - \sum_{i=0}^{k-1} \frac{\binom{M}{i}\binom{N-M}{n-i}}{\binom{N}{n}}$$

In this equation, N is the total number of genes in the background distribution. In contrast, M represents the number of genes directly or indirectly related to the gene set of interest. In addition, n indicates the size of the list of genes of interest, and k represents the number of genes within the list that are annotated to the gene set. The cut-off threshold was determined to be *p*.adjust < 0.05. GSEA was conducted to identify significantly enriched gene sets associated with the biological conditions under investigation. The analysis was performed using GSEA version 4.0.2.

2.5 Survival analysis

Survival analysis was performed to explore whether the co-expressed genes were associated with the prognosis of GC patients. The log-rank test for survival analysis was used to analyse the influence of multiple variables on time-to-event outcomes, such as mortality. The Kaplan–Meier survival curve was defined as the chance of survival at a given time. The patients were assigned to two groups according to the median expression of notable GC-related genes. Univariate Cox regression analysis revealed that significant survival-related genes are potentially functional in gastric adenocarcinoma. The difference in survival rates between the high- and low-risk groups was determined through Kaplan–Meier analysis, with a log-rank test using the R package surfminer. The survival probability was calculated by the survival time, survival state, and different grouping conditions as follows: $S(t) = P(T > t) = 1 - F(t), 0 < t < \infty$.

The Kaplan–Meier plot can be interpreted as a step function, with a vertical drop in the curve indicating a death event. The survival package's survfit function calculates the Kaplan–Meier estimator for truncated and/or censored data. The left-hand side of the formula is a Surv object, and the right-hand side contains various categorical variables that group the observations. The hazard ratio, with 95% confidence intervals, and log-rank *p* values were computed, and *p*-values less than 0.05 were regarded as statistically significant.

2.6 Transcription factor binding site prediction

We used the transcription factor binding site (TFBs) footprint method to computationally predict the TFBs of the candidate prognostic genes of interest. We employed 575 position weight matrices based on binding data from the JASPAR database. TFBs footprinting used a 'pb' value of 1000 for gene transcript prediction, with all other parameters set to their default values. Published data on genes and their transcription factors were collected, and the transcription factors of target genes were predicted utilising prediction tools (https://tfbs-footprinting.readthedocs.io/en/latest/intro.html#basics).

2.7 GC cell culture and treatment

The human GC cell line MKN-45 was a gift from the Cancer Hospital Chinese Academy of Medical Science (Beijing, China). The cell line was cultured in Dulbecco's modified Eagle's medium (DMEM)/F12 supplemented with 10% foetal bovine serum, 100 U/ml penicillin, and 100 µg/ml streptomycin (standard DMEM/F12). BATF2 siRNAs (30 pmol) (OBiO Scientific Service, Beijing, China) were transiently transfected into GC cell MKN-45 utilising a Lipofectamine 3000 Transfection Kit (L3000-008, Invitrogen, Carlsbad, CA, USA). After transfection, the cells were cultured for 24 h and collected for further analysis.

2.8 Animal studies

Five-week-old 615 mice were purchased from the Institute of Haematology and Blood Diseases Hospital (Chinese Academy of Medical Sciences & Peking Union Medical College, Tianjin, China). All the animals were acclimated under standard laboratory conditions and had free access to standard water and food. All procedures were conducted in accordance with the Guiding Principles in the Care and Use of Animals (China) and were approved by the Laboratory Animal Ethics Committee of Beijing YongXinKangTai Technology Development Co., Ltd (Refinement No. YXKT2022L018). Mouse MFC cells (4 * 10^6 cells/200 µL) were subcutaneously injected near the forelimb of mice, and the primary tumour tissue was collected as it reached 1000 mm^3 for further in vivo model. For the in vivo anti-PD-1 treatment model, the primary tumour tissue was cut in pieces of 10 mm^3 and subcutaneously embedded near the mice's forelimb. When the tumour volume reached 100–150 mm^3, 200 µg mouse anti-PD-1 antibody (anti-mPD1) (BE0146, Bio X Cell) or IgG control (BE0089 Bio X Cell) was injected intraperitoneally in the mice 4 times at 3-day intervals, then the tumours were harvested for the further experiment.

2.9 RT-qPCR

RT-qPCR was performed to assess the knockdown levels of BATF2 in the human GC cell line MKN45. Briefly, RNA concentration was determined utilising a Nanodrop device (Thermo Scientific), and complementary DNA (cDNA) was synthesised employing a HiScript III RT SuperMix kit (Vazyme Biotech), strictly adhering to the guidelines provided by the manufacturer. Quantitative PCR was conducted on a CFX96 Real-Time System (Bio-Rad Laboratories, Hercules, CA) using ChamQ Universal SYBR Green Master Mix (Vazyme Biotech). The amplification protocol included specific primers for human BATF2 (forward primer: TCAGGGAAGCCAAGTGACAAGTC, reverse primer: ACAGGAGAAGGAGGAGCAGAGG). The gene expression levels were denoted as the number of copies per microgram of total RNA. The relative expression quantification was executed utilising the comparative 2-ΔΔCt method, with GAPDH serving as the normalisation reference for cDNA.

2.10 MTT assay

The viability of the cancer cells was evaluated using the MTT assay. The siRNA-transfected cells were seeded in 96-well plates with a final volume of 100 µl. At 24–72 h, 5 mg/ml MTT reagent (10% v/v, without replacing the medium) was added to each well, and after 3-h incubation, the medium was removed, and 200 µl of DMSO was added. The plate was placed on a shaker to dissolve the formazan crystals. The absorbance was measured using a SpectraMax M5® microplate reader (Molecular Devices, California, USA) with a reference wavelength of 490 nm.

2.11 Enzyme-linked immunosorbent assay (ELISA)

Protein extracts from human GC cells, MKN-45, primed with siRNA were prepared using RIPA buffer, and the concentrations of proliferation markers and PD-L1 were tested by Human CCNB1 ELISA kit (Cat. No. MM-610052H1) and Human CCND1 ELISA kit (Cat. No. MM-0404H1), Human PD-L1 ELISA kit (Cat. No. MM51811 h1), according to the manufacturer's instructions. All ELISA kits were purchased from Meimian Industrial Co., Ltd. (Jiangsu, China).

2.12 Western blotting

Primary gastric cancer tumour tissue lysates were prepared in RIPA lysis buffer containing 2% (v/v) protease inhibitor cocktail and 1% (v/v) phosphatase inhibitor on ice. Protein concentration was determined using a BCA protein assay kit (Pierce, USA). Total protein (30 µg) was separated by 10% SDS-PAGE and transferred onto a PVDF membrane (Merck Millpore). After blocking the membrane with 5% milk for 2 h at room temperature, primary antibodies were incubated overnight at 4 °C with continuous gentle rolling: anti-β-actin (1:50,000, AC026, ABclonal); anti-BATF2 (1:1000, 16,592-1-AP, Proteintech). The membrane was then incubated with the enzyme-conjugated secondary antibody peroxidase AffiniPure donkey Anti-Rabbit IgG (1:10,000, ZB-2301, Zsbio) for 2 h at room temperature. A chemiluminescence kit was employed to visualise immunocomplexes using a chemiluminescence imaging system. The Image J software (Syngene, UK) was employed to quantify the bands, and the level of actin was used to normalise the data.

2.13 Statistical analysis

Group comparisons were conducted utilising either Student's *t*-test or analysis of variance for further analysis (GraphPad Prism for Apple Macintosh, version 9). The results are reported as the mean ± standard deviation (SD) unless otherwise stated. Statistical significance was defined as *p*-values equal to or less than 0.05.

3 Results

3.1 Identification of differentially expressed mRNAs in human GC tissues

Differentially expressed genes (DEGs) analysis was initially conducted for GC and adjacent to cancer. Data on 375 GC samples and 32 normal samples were obtained from the TCGA database, and 7467 differentially expressed mRNAs were identified (Fig. 1, panel A). Moreover, the cut-off points were set in advance, with a fold change > 1.5 and p value < 0.05, to screen significantly differentially expressed mRNAs. As shown in Fig. 1 (panels B and C), 3587 (48.04%) of the 7467 DEGs were significantly upregulated, and 3878 (51.94%) were significantly downregulated.

Next, 2295 genes were analysed to evaluate the correlation between PD-L1 (CD274) and other genes in the TCGA database. The genes with a p-value < 0.05 were selected, of which 2073 and 222 showed positive and negative correlations, respectively. To identify co-expressed genes, the top 500 PD-L1 co-expressed genes were selected based on the Pearson correlation coefficient, ordered in descending value (the co-expression pattern of the top nine gastric adenocarcinoma genes with PD-L1 is shown in Supplementary Fig. 1). An intersection analysis was conducted to better understand the interplay between the 7465 DEGs and the top 500 co-expressed genes, and 189 DEGs were found to be co-expressed with PD-L1 in GC. Interactions between these 189 candidate genes were constructed using a curated database, and the degree of each node was calculated using STRING (https://string-db.org/, version 12) (Fig. 1, panel D). Forty-seven genes were excluded because they did not interact with other genes. The node degrees of the top 30 genes are shown in Supplementary Table 1.

3.2 DEGs co-expressed with PD-L1 are enriched in immune-associated biological processes and signalling pathways

To understand the biological functions and processes of the 142 DEGs co-expressed with PD-L1 in gastric adenocarcinoma, we analysed the signalling pathways enriched by these genes. Several immune- and inflammatory-modulatory processes were significantly enriched, including the 'Cytokine-cytokine receptor interaction', 'Chemokine signalling pathway', 'Toll-like receptor signalling pathway', 'NOD-like receptor signalling pathway', 'Th1 and Th2 cell differentiation' and 'B cell receptor signalling pathway'. In addition, GSEA results suggested that pathways of the 'NF-kappa B signalling pathway', 'HIF-1 signalling pathway', 'C-type lectin receptor signalling pathway' and 'PD-L1 expression and PD-1 checkpoint pathway in cancer' tended to be activated in the cancer group (Fig. 2A and Supplementary Fig. 2). GO analysis revealed that the changes in the 'Biological Process' (BP) of DEGs co-expressed with PD-L1 were enriched in the 'immune response', 'inflammatory response', 'chemokine-mediated signalling pathway, 'T cell activation', and 'T cell co-stimulation';

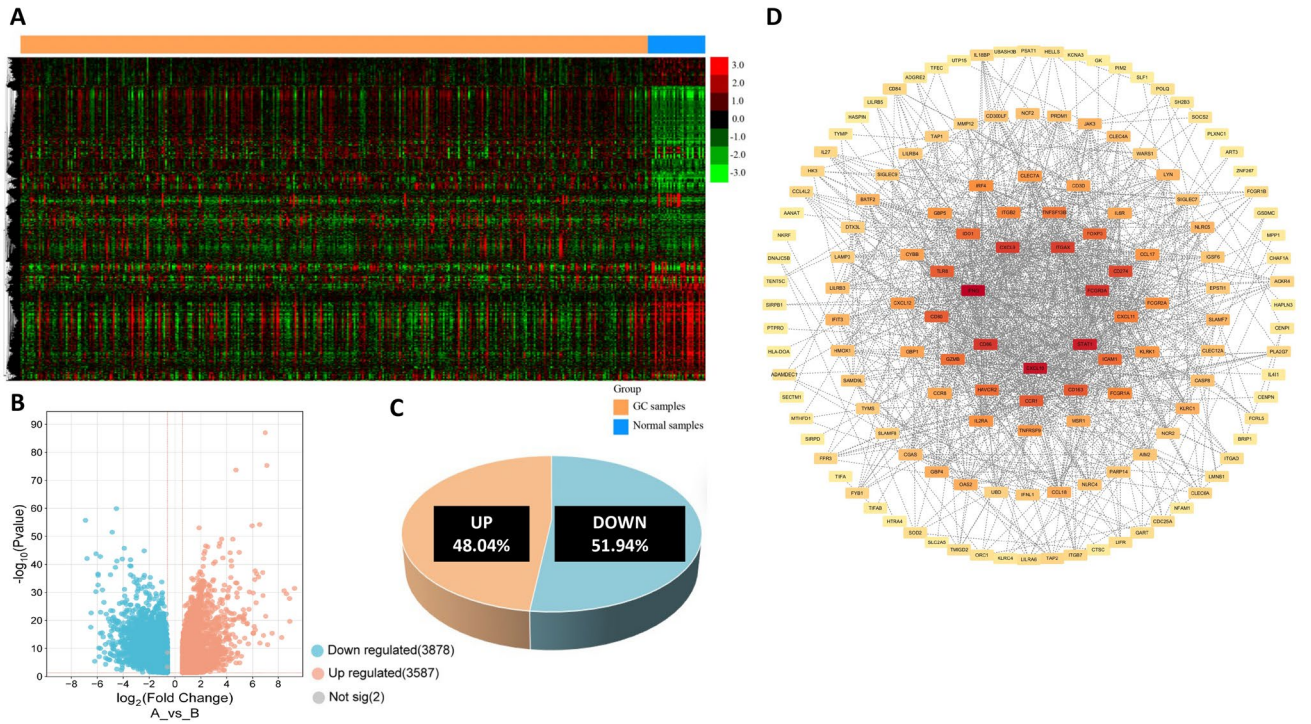

Fig. 1 Overview of 142 differentially expressed genes co-expressed with PD-L1 in GC. **A** Heatmap showing the differentially expressed mRNAs in tissues from GC and adjunct to cancer from TCGA database. The data on each row represents the genes (n = 7467), and each column indicates the samples. Red and green indicate upregulated expression (n = 3587) and downregulated expression (n = 3880), respectively. Colour density indicates the levels of fold change. **B** Volcano plot illustrating the differentially expressed mRNAs in tissues from GC and adjunct to cancer. The X-axis is $\log_2$(Fold change) of gene expression levels between cancer and normal tissue, and the Y-axis is the *p*-value based on −log10. The coloured dots on the left (blue) and right (orange) represent genes with downregulated and upregulated expression, respectively, based on a *p*-value < 0.05 (the red horizontal line) and a 1.5-fold change expression difference (the two red vertical lines). **C** Pie chart depicting the total number of differentially expressed genes with upregulated, downregulated, or ambiguous expression. **D** PPI network graph constructed in STRING. Edges indicate functional and physical protein associations; nodes represent genes, and lines connecting genes represent interactions. Minimum required interaction score: high confidence (0.7). Disconnected nodes are hidden in the network

the changes in the 'Cellular Components' (CC) was enriched in 'plasma membrane', 'external side of plasma membrane', and 'immunological synapse'; and the changes in the 'Molecular Function' (MF) was enriched in 'protein binding', 'signalling receptor activity', 'transmembrane signalling receptor activity', and 'chemokine activity' (Fig. 2, panel B). GO and KEGG analyses were primarily conducted on pro-inflammatory and immune-related pathways. As shown in Fig. 2, 56 and 62 DEGs co-expressed with PD-L1 were significantly concentrated in twenty signalling pathways (panel C) and ten biological processes (panel D), respectively. Intersection analysis showed that 41 DEGs co-expressed with PD-L1 were enriched in immune-associated biological processes and signalling pathways.

3.3 Altered expression of immunotherapy response gene BATF2 is associated with overall survival in GC patients

To test whether the 41 candidate genes were positively responsive to anti-PD-1 immunotherapy in GC patients, DEGs analysis was conducted on clinical samples obtained from immunotherapy responders and non-responders in the PRJEB25780 Dataset. Twenty-one and 57 clinical samples that positively and negatively responded to anti-PD1 immunotherapy were obtained from the STAD-PRJEB25780_anti-PD-1 dataset. Additionally, 2399 differentially expressed mRNAs that respond to anti-PD1 immunotherapy between the responder and non-responder groups were identified based on a *p*-value < 0.05. Moreover, the cut-off points were set in advance, with fold change > 1.5 and *p*-value < 0.05, to filter out significantly differentially expressed mRNAs. As shown in Fig. 3 (panel A), 137 (5.7%) significantly upregulated DEGs are positive responses in anti-PD1 immunotherapy, and 89 (3.7%) downregulated DEGs are negative responses in anti-PD1 immunotherapy. The top 100 DEGs are shown in a heatmap (Fig. 3, panel B). To better understand the interplay between

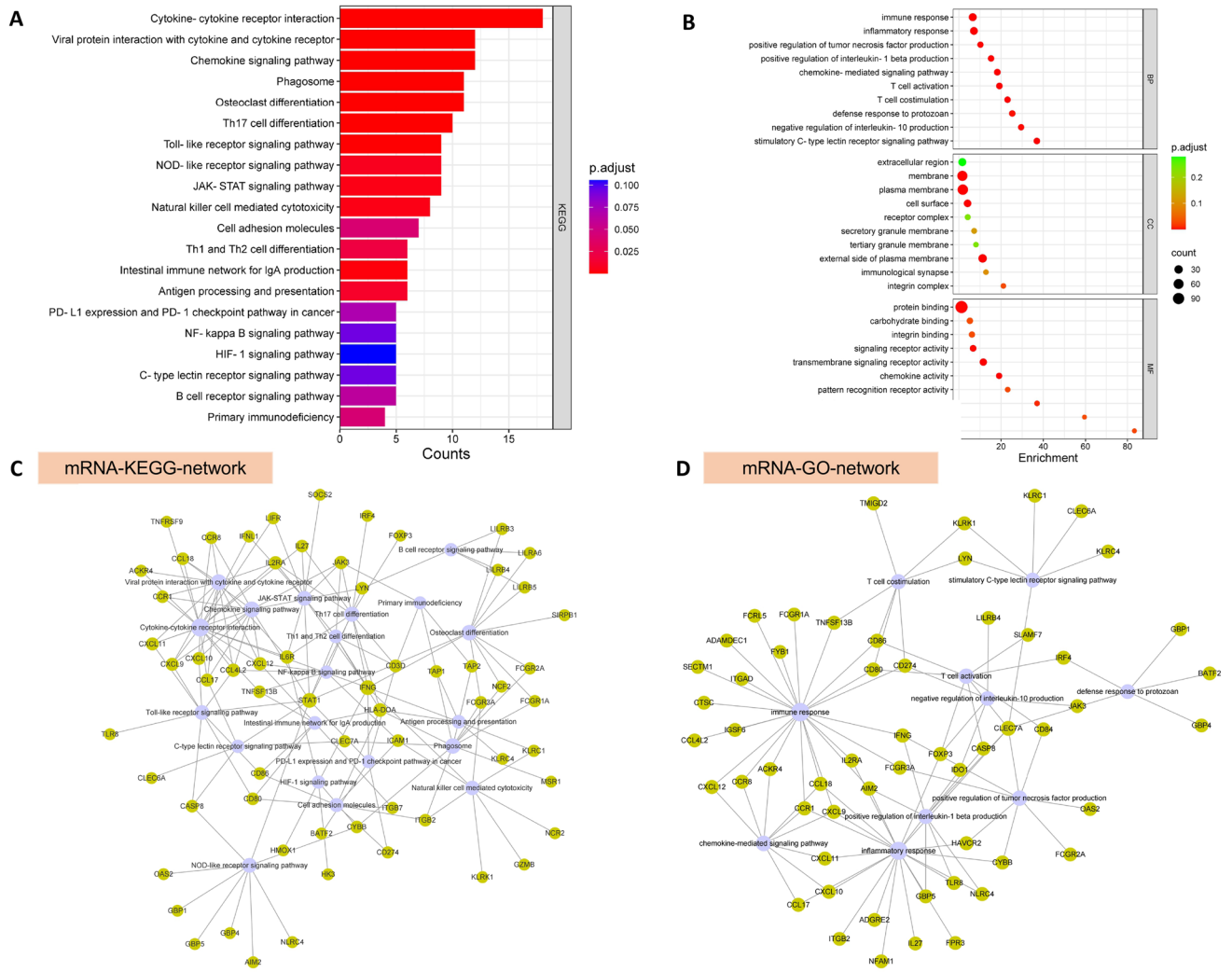

Fig. 2 GO and KEGG pathway enrichment and network analysis of 142 DEGs co-expressed with PD-L1. **A** Bar chart depicting the 20 significant pathways in the KEGG analysis. **B** The bubble chart shows the 10 significant items in the BP, CC, and MF sections according to the adjusted *p*-values in the GO analysis. The adjusted *p*-value represents the degree of significant fold enrichment. The number of genes observed in a pathway corresponds to the size of the circle. **C** The functionally grouped network was visualised using Cytoscape based on the degree of connectivity between pathways and genes. **D** The functionally grouped network was visualised using Cytoscape based on the degree of connectivity between GO terms and genes

the 41 candidate genes and the 226 immunotherapy response-associated genes, an intersection analysis was conducted to obtain nine up-regulated DEGs positively responding to anti-PD1 treatment in GC patients (Fig. 3, panel C). The details of the nine candidate genes in the anti-PD1 immunotherapy responder group are listed in Supplementary Tables 2 and 3. Next, Kaplan–Meier survival curves were generated to examine whether the alteration of these nine candidate genes was associated with a poor prognosis of GC. As shown in Fig. 3 (panel D), only BATF2 significantly affected the overall survival of patients in the log-rank test. The overall survival of GC patients was found to be improved with high BATF2 expression ($p < 0.05$) (the overall survival log-rank *p*-value of the other eight candidate genes for GC survival is shown in Supplementary Fig. 3).

3.4 Downregulation of BATF2 enhances the ability to promote in vitro growth and tumour immune escape in human GC cells

To determine the signature of the candidate gene, BATF2, transcriptomic profiling analysis was conducted on clinical samples obtained from the Tumour Immunotherapy Gene Expression Resource (TIGER) dataset. The Single-Cell Immunity Datasets of TIGER were used to analyse the cells from clinical samples of non-atrophic gastritis (NAG) (n = 3), chronic

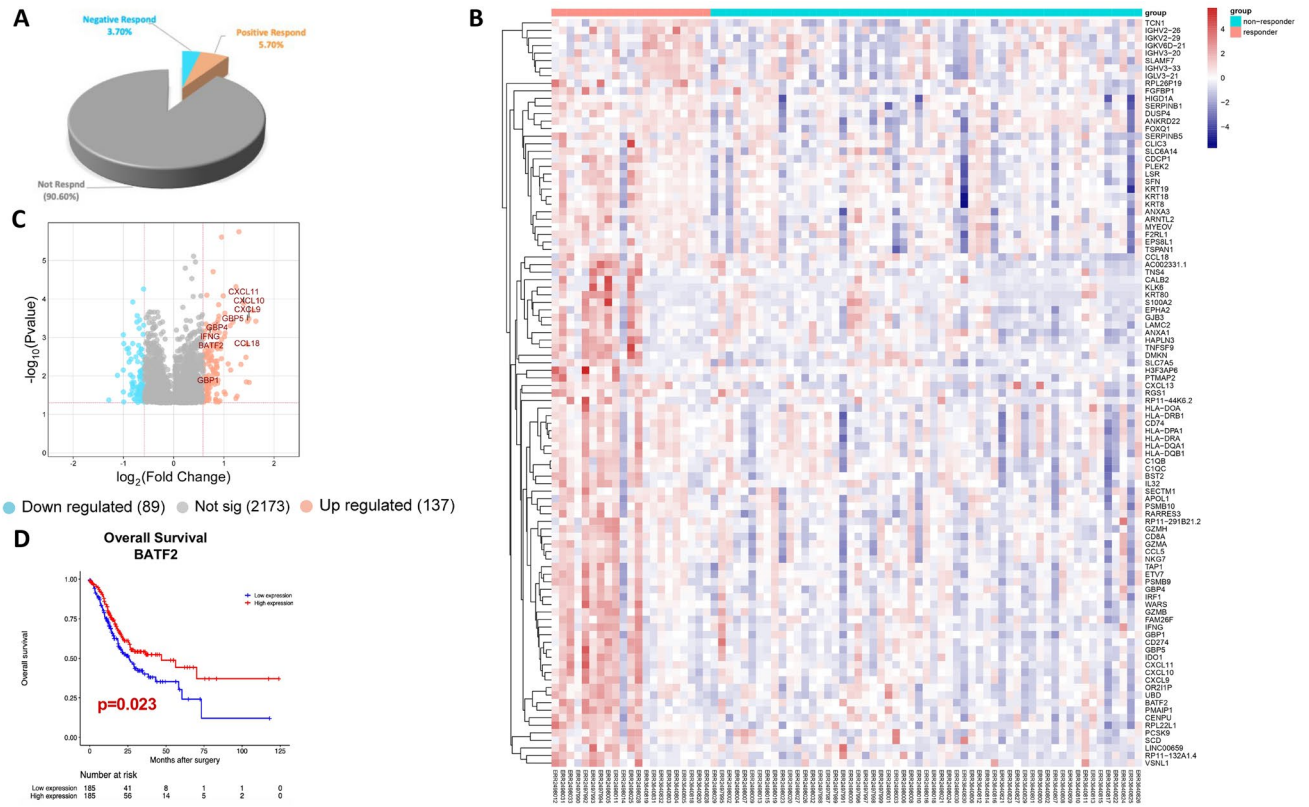

Fig. 3 Candidate gene BATF2 is of significant prognostic value for anti-PD1 immunotherapy in GC patients. **A** Pie chart depicting the number of differentially expressed genes with positive, negative, and no responses. **B** Heatmap illustrating the positive response genes from the positive and negative responder groups. The data on each row represents the genes (n = 100), and each column indicates the clinical samples. Red and blue indicate upregulated and downregulated expression in the immunotherapy responder group, respectively. **C** Volcano plot showing the differentially expressed mRNAs in tissues from positive- and negative-anti-PD-1 immunotherapy groups. The X-axis is $\log_2$(Fold change) of gene expression levels between the responder and non-responder groups, and the Y-axis is the *p*-value based on −log10. The coloured dots on the left (blue) and right (orange) represent genes with negative and positive responses based on a P-value < 0.05 (the red horizontal line) and a 1.5-fold change expression difference (the two red vertical lines). **D** Kaplan–Meier overall survival plots for GC patients from the TCGA database (n = 370), comparing those with low (blue line) and high (red line) expression levels of BATF2. The low- and high-expression groups were divided by the median expression level of genes

atrophic gastritis (CAG) (n = 2), intestinal metaplasia (IM) (n = 4), and GC tumours (n = 1) to characterize the candidate gene BATF2 precisely. The literature on this dataset details the collection and processing of clinical samples, the post-quality control assessment (Supplementary Fig. 4, panel A), and the transcriptomic data collection and processing steps of 33,219 individual cells [19]. The cell clusters were annotated with the dominant expression pattern of specific cell markers. Nine cell types were identified via UMAP analysis: malignant cells, endocrine cells, B cells, fibroblasts, T cells, goblet cells, and endothelial cells (Fig. 4, panels A and Supplementary Fig. 4, panel B). To further explore BATF2 expression, differential expression was analyzed between tissue samples from GC and gastritis tissues in TIGER datasets based on a logarithmic scale (base 2) fold change value. The data showed that BATF2 is mainly distributed in endothelial (log (FC) = 0.0298), fibroblast (log (FC) = 0.0310), malignant (log (FC) = −0.0044), and endocrine cells (log (FC) = −0.0013) (Fig. 4, panel B). Although the candidate gene BATF2 is mainly expressed in endothelial cells, the primary sources of endothelial cells were CAG (53.66%, 16,025 individual cells), IM (40.59%, 9791 individual cells) and NAG (5.25%, 6209 individual cells) rather than GC (0.5%, 1194 individual cells) (Supplementary Fig. 4, panel C). GEPIA violin plot of gene expression by pathological stages based on the TCGA clinical annotation indicated the low expression levels associated with the advanced TNM stage (Supplementary Fig. 4, panel D). Furthermore, the single cell-sequencing data indicated that the candidate gene BATF2 was mainly expressed in endocrine cells (log (FC) = 0.007), malignant cells (log (FC) = 0.005), and fibroblast cells (log (FC) = 0.028) of GC tissues when compared to gastritis tissues (Fig. 4, panel C). The distribution difference of BATF2 analysis in GC tissues showed that BATF2 expression accounted for 10.09%, 3.61%, and 0.56% in endocrine, malignant, and fibroblast cells, respectively (Fig. 4, panel D and Supplementary Fig. 4, panel E).

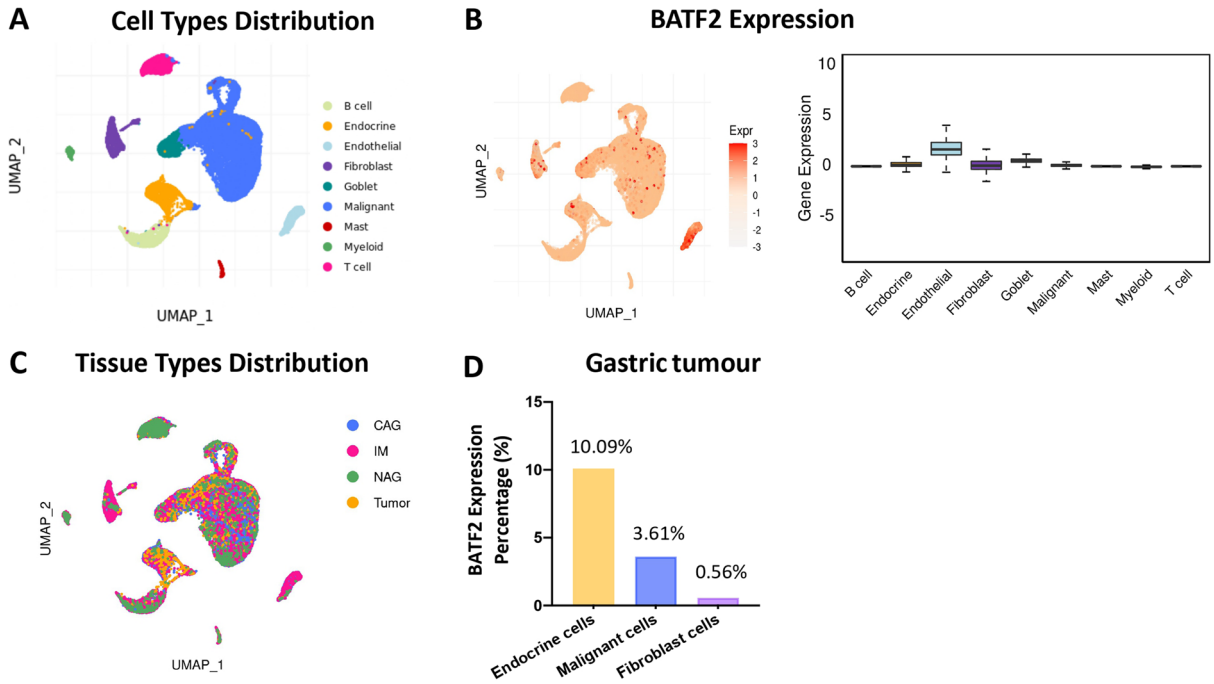

Fig. 4 Candidate gene BATF2 is mainly distributed in the endocrine and malignant cells in the single-cell profile of clinical samples from gastric tumours. **A** Examination of RNA-seq data sets from clinical samples reveals the presence of nine cell types. **B** UMAP plots and quartiles for box plots reveal the distribution and proportion of candidate gene BATF2 in different cell types. **C** UMAP plots reveal the distribution of clinical GC and gastritis tissue samples in different cell types. **D** Bar chart reveal the proportion of candidate gene BATF2 in different cell types of clinically GC tissue samples

BATF2 is a tumour suppressor that inhibits cancer cell growth [20]. Guided by previous data, we performed experiments to test if BATF2-knockdown can affect the proliferative ability of human GC cells MKN-45. As shown in Fig. 5, the siRNA constructs knocked down BATF2 expression by 15% ($p < 0.05$) and 28% ($p < 0.05$) for $BATF2^{KD321}$ and $BATF2^{KD568}$ (Panel A), respectively. Further analysis of cell viability in cultures exposed to these targeting constructs revealed that the addition of $BATF2^{KD321}$ and $BATF2^{KD568}$ significantly increased the growth of human GC cells MKN-45 when compared to that in the NC-treated group (Fig. 5, Panel B). As shown in Fig. 5 (Panel C-D), the proliferation marker genes (CCNB1 and CCND1) were upregulated in MKN-45 cells after being primed with the $BATF2^{KD321}$ and $BATF2^{KD568}$ constructs. Furthermore, the BATF2 mRNA-targeting constructs showed an inverse correlation with the expression of PD-L1. Cultures exposed to $BATF2^{KD321}$ and $BATF2^{KD568}$ significantly increased PD-L1 expression (Fig. 5, Panel E). Furthermore, the mouse anti-PD1 was administrated after embedding the mouse GC cells MFC-formed tumour tissues. As seen in Fig. 5 (Panels F), parental GC tumours were significantly positively responsive to anti-mPD1 treatment, as evidenced by a reduction in tumour growth compared to that exposed to IgG Control. The tumour tissue sensitive to anti-PD1 administration caused a significant increase in BATF2 expression ($p < 0.05$) when compared to primary tumour tissues (Fig. 5, panel G).

To gain further insight into the synergistic effects of BATF2 and PD-L1 in selecting GC patients for PD-L1 inhibitor immunotherapy, we performed transcription factors (TFs) prediction analyses for the candidate gene BATF2 to discover additional potential predictors and therapeutic targets for GC. TFs are a class of sequence-specific DNA-binding proteins that can bind to the sequence of TF-binding sites upstream of target genes and regulate gene transcription. As they play an essential role in tumour development, targeting these TFs may directly impair the survival and dissemination of tumour cells [21]. Our data showed that STAT and IRF family members were predicted as binding proteins of BATF2. This finding is consistent with immunoprecipitation studies showing that BATF2/IRF1 is likely to regulate the expression of immune effector genes cooperatively [22]. The top ten predictions of BATF2 are listed in Table 1. These TFs can directly regulate the expression of PD-L1-related genes, which may indirectly affect PD-L1 expression. Thus, these TFs may also serve as potential therapeutic targets.

4 Discussion

The emergence of the PD-1/PD-L1 immune checkpoint as a marker for predicting diagnosis and treatment efficacy has revolutionised cancer treatment, effectively providing treatment opportunities for a wide range of cancer types. Nivolumab was the first anti-PD-1 mAb to show a significant prolonged OS in patients with GC [23]. It also demonstrates improved OS in patients with advanced gastric adenocarcinoma when compared to chemotherapy alone [24]. In addition, nivolumab exhibits anti-tumour efficacy in metastatic melanomas and non-small-cell lung carcinoma [25, 26]. It also has shown promising effects in individuals with relapsed or refractory Hodgkin's lymphoma [27]. Pembrolizumab has shown significant clinical activity and has been approved by the USA for treating patients with metastatic GC [28]. The phase III KEYNOTE-859 trial elucidates its function as a first-line therapeutic option for patients with HER2-negative advanced GC [29]. In addition, pembrolizumab exerts significant therapeutic efficacy in some solid tumours, such as bladder cancer [30], classical Hodgkin's lymphoma [31] and triple-negative breast cancer [32].

The immune microenvironment plays a significant role in determining the effectiveness of immunotherapy, as it encompasses a complex interaction between immune cells, tumour cells and other stromal components. Accumulating immunosuppressive cells such as regulatory T cells (Tregs) and myeloid-derived suppressor cells (MDSCs) in the tumour microenvironment has profound implications for immune evasion and tumour progression. In gastric adenocarcinoma, high levels of Tregs in the tumour tissue and peripheral blood have been linked to poor prognosis, as they create an immunosuppressive niche that inhibits the activity of CD8 + cytotoxic T cells, thereby reducing the clinical activity of PD-1/PD-L1 inhibitors [33]. MDSCs contribute to tumour-associated angiogenesis by secreting pro-angiogenic factors such as vascular endothelial growth factor (VEGF), which helps tumours grow and spread. The crosstalk of MDSCs and immune cells (macrophages and dendritic cells) within the tumour microenvironment contributes to an immunosuppressive environment that promotes tumour survival. Tregs can further inhibit the activation of T cells and promote the accumulation of MDSCs by secreting anti-inflammatory cytokines, such as IL-10 and TGF-β. This creates a double barrier to suppress antitumour immunity in the microenvironment. The combination of Tregs, MDSCs, and immunosuppressive cytokines leads to an overall suppression of the immune system in GC [34]. To improve immune responses in cancer, the combination of PD-1/PD-L1 blockade and treatments targeting Treg or MDSCs is being explored to restore the activity of tumour-specific T cells and enhance the therapeutic effects of PD-1/PD-L1 inhibitors. For instance, combining PD-1/PD-L1 inhibitors with Treg-depleting antibodies or VEGF antibodies has enhanced immune response in head and neck squamous cell carcinoma and breast cancer [35, 36].

However, in GC patients, the PD-1/PD-L1 expression level in tumour cells or surrounding immune cells is low, and PD-1/PD-L1 expression can sometimes yield false positives. Thus, PD-1/PD-L1 single-target blockade therapy is often ineffective [14, 37]. The emerging role of biomarkers in guiding immunotherapy for gastric adenocarcinoma is pivotal in advancing personalised cancer treatments. Gastric cancer, particularly in its advanced stages, is a heterogeneous disease, and its response to immunotherapy varies significantly among patients. This variability underscores the importance of biomarker screening to guide patient selection. Consequently, screening biomarkers related to PD-1/PD-L1 for targeted and individualised treatment of GC patients is necessary. PD-1/PD-L1-related biomarkers can predict the expression level of checkpoints in combination with PD-L1 and aid in selecting effective inhibitors for treatment. Still, they may also serve as therapeutic targets to enhance the benefits of combination therapy with PD-1/PD-L1 inhibitors.

In recent years, several biomarkers, such as PD-L1 expression, microsatellite instability (MSI), and tumour mutational burden (TMB), have played an essential role in identifying which patients with gastric cancer are most likely to benefit from immune checkpoint inhibitors. PD-L1 expression measured by combined positive score (CPS) or tumour proportion score (TPS) is the most reliable predictive factor to identify GC patients eligible for treatment with PD-1/PD-L1 inhibitors. The data indicate that the efficacy of PD-1 blockade in gastric adenocarcinoma is associated with a higher CPS of PD-L1 expression and a promising clinical benefit of immunotherapy in selected GC patients with CPS ≥ 5 [38]. As for PD-L1 positive tumours in the meta-analysis of seventeen phase III clinical trials, the overall survival in PD-L1 positive patients was longer than that of PD-L1 negative patients with advanced GC [39]. In the phase II KEYNOTE-059 trial, the PD-L1 positive tumour with CPS ≥ 1 and PD-L1 negative tumour with CPS < 1 demonstrated an objective response rate (ORR) of 22.7% and 8.6%, respectively [9]. The phase III KEYNOTE-061 trial suggested that advanced GC patients with high PD-L1 expression (CPS ≥ 10) benefited more from pembrolizumab treatment [40]. Tumours with high MSI show a dense infiltration of CD8 + lymphocytes, which can trigger a more robust immune response. As for MSI in the meta-analysis, the ORR and disease control ratio of anti-PD-1 therapy in MSI-high GC

Fig. 5 BATF2 mRNA-targeting constructs enhanced the growth and the immune escape ability of human MKN-45 GC cells in vitro. **A** qPCR ▶ quantification of the differential expression of BATF2 mRNA expression in cell lysates obtained from the mock control or MKN-45- $BATF2^{KD}$ GC cells. **B** After treatment with si-RNA for 24 h, MKN-45 cells were further cultured. Cell viability was assessed with MTT. **C–E** Protein levels of proliferation markers (CCNB1 and CCND1) and PD-L1 in si-BATF2-treated MKN-45 cells. **F** Scatter dot plots of individual data points and representative images of tumour tissues showing the changes in tumour volume in MFC-P-tumour-bearing mice treated with anti-PD1 or IgG. N = 9 for each group. **G** Western blot quantification represents the BATF2 expression. The blots were analysed for the indicated antibody, and anti-rabbit β-actin was used as the loading control. In vitro results are from three independent experiments. Values are presented as mean ± SD from three independent experiments (*$p < 0.05$, **$p < 0.01$, ***$p < 0.001$)

patients was significantly higher than that of microsatellite-stable GC patients [41]. In the meantime, the PD-1 inhibitor, pembrolizumab, works better for patients with metastatic GC whose tumours have an MSI of high [42]. In addition to these, TMB is also a promising biomarker for immunotherapy. The high TMB demonstrates an increasing benefit of immune checkpoint inhibitor treatment in GC [43]. Therefore, biomarker screening is essential in selecting individuals with gastric adenocarcinoma who are most likely to benefit from immunotherapy.

This study aimed to identify PD-L1-related biomarkers that could improve patient selection for PD-1/PD-L1 inhibitor therapy. PD-L1 expression, combined with other potential biomarkers, may have a higher predictive value for response to immune checkpoint inhibitors than an individual biomarker. 7467 DEGs were found in GC tissues and adjacent to cancer tissues from the TCGA database, and 2295 genes were associated with PD-L1 expression. Among the top 500 PD-L1 co-expression genes, 125 genes were differentially expressed in gastric adenocarcinoma tissues and adjacent to cancer tissues. A PPI network was constructed, and 47 genes were excluded because they did not interact with other genes. GO and KEGG analyses were performed to assess the primary function of 142 genes. Most of these 142 genes were classified into functional categories related to immune function and cancer pathways. Forty-one genes were identified based on the intersection of the mRNA-significant GO term network and the mRNA-significant signalling pathway network. Additional intersection analysis of 41 candidate genes and 226 positive immunotherapy response genes yielded nine candidate genes. We generated Kaplan–Meier survival curves to explore the potential roles of these nine genes in the overall survival of GC patients. Only BATF2 was demonstrated to have a significant effect on patients'overall survival and high expression of BATF2 was associated with better overall survival. However, public datasets come with inherent biases and limitations, such as demographic representation, clinical subtypes of cancers, bias in tumour heterogeneity, lack of long-term follow-up and lack of direct translation to functional biological of genomic and transcriptomic insights for TCGA datasets. In datasets like TIGER, the limitation of the applicability of the findings to fewer types of cancers and the lack of detailed immune profiling limit the ability to study tumour-immune interactions accurately. Therefore, the functional assays were conducted to determine the role of BATF2 in GC. We conducted experiments on the effects of gene knockdown on GC cell growth. We found that BATF2 is closely related to PD-L1 and thus can serve as a biomarker—a potential target for immune checkpoint blockade therapy. Additionally, TF predictions for BATF2 were also performed, and our data suggested that STAT and IRF family members are the principal TFs for BATF2 and have the potential to be key biomarkers for adjuvant therapy.

In this study, we observed an interesting phenomenon; this factor is theoretically highly expressed in tumour tissues and is generally considered an oncogene that promotes tumour occurrence and development [44, 45]. However, the BATF2 identified through our screening exhibited unique characteristics; BATF2 is typically upregulated in GC tissues. However, the survival analysis revealed that the overall survival of GC patients with high BATF2 expression was longer. BATF2 is stably expressed in various normal cells but is dysregulated in tumour cells [46–48], which can suppress the growth and spread of tumour cells and induce apoptosis [47, 49, 50]. These findings are consistent with previous in vitro studies showing that GC cells with low BATF2 expression significantly promoted proliferation. The downregulation of BATF2 expression in GC tissues affects the transcription of certain classical T-cell activation genes (IFNG, GZMB, PRF1, and TNF). It ultimately inhibits the activation of CD4 + memory T cells, forming an immunosuppressive microenvironment that promotes the occurrence and development of GC [51]. BATF2 overexpression significantly increases p53 tumour suppressor protein levels, inhibiting ERK signalling to reduce GC growth and metastasis [20]. The antitumour effect of BATF2 is reflected in GC and plays a role in other tumours. Liu et al. showed that BATF2 inhibits the expression of PD-L1 by suppressing ZEB2 in the PI3 K/AKT signalling pathway and enhancing the infiltration and activation of CD8 + T cells. ZEB2 can induce tumour cells to express PD-L1 and then evade immune surveillance. BATF2 is negatively correlated with the expression of PD-L1 in NSCLC patients, and BATF2 inhibits PD-L1 expression at both the mRNA and protein levels [52]. BATF2 prevents glioblastoma multiforme progression by inhibiting the recruitment of myeloid-derived suppressor cells [53]. The decreased BATF2 expression is associated with an inferior outcome in hepatocellular carcinoma and oral tongue squamous cell carcinoma [54, 55]. Moreover, BATF2 inactivates HGF/MET signalling in colorectal cancer, and

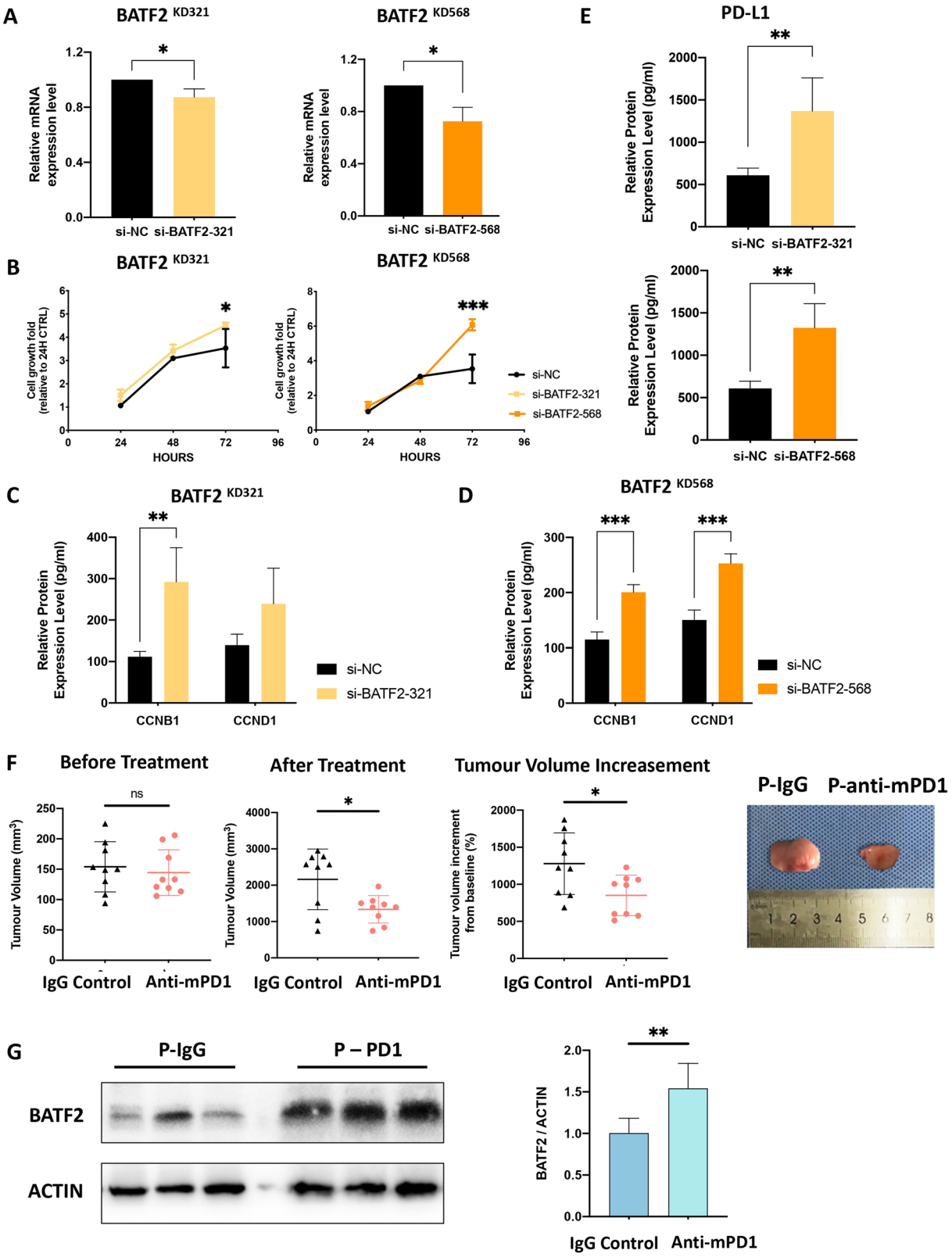
A
BATF2 KD321
Relative mRNA expression level
si-NC si-BATF2-321
BATF2 KD568
si-NC si-BATF2-568
E
PD-L1
Relative Protein Expression Level (pg/ml)
si-NC si-BATF2-321
si-NC si-BATF2-568
B
BATF2 KD321
Cell growth fold (relative to 24H CTRL)
HOURS
BATF2 KD568
si-NC
si-BATF2-321
si-BATF2-568
C
BATF2 KD321
CCNB1
CCND1
si-NC
si-BATF2-321
D
BATF2 KD568
si-NC
si-BATF2-568
F
Before Treatment
After Treatment
Tumour Volume Increasement
Tumour Volume (mm³)
Tumour volume increment from baseline (%)
IgG Control Anti-mPD1
P-IgG P-anti-mPD1
G
P-IgG P – PD1
BATF2
ACTIN
BATF2 / ACTIN
IgG Control Anti-mPD1

Table 1 Top 10 transcription factor predictions of candidate genes

Rank	Binding protein	Motif	*p*-value
BATF2			
1	IRF8	GAGAAACTGAAACT	1.00E−06
2	CTCF	AGGCCTCCAGAGGGCACTG	1.00E−06
3	STAT1::STAT2	CAAGTTTCAGTTTCT	1.00E−05
4	IRF5	GAGAAACTGAAACT	1.00E−05
5	USF2	CTTGCTCACGTGGCTA	1.00E−05
6	CTCFL	CTCCAGAGGGCACT	1.00E−05
7	CTCF	AGGCCTCCAGAGGGCACTG	1.00E−05
8	USF2	CTTGCTCACGTGGCTA	1.00E−05
9	IRF1	GCCAAGTTTCAGTTTCTCCTA	1.00E−05
10	NR1H3::RXRA	TGCCCTCTGGAGGCCTAAG	1.00E−04

HGF/MET signalling is frequently activated in various human malignancy fields [56]. Taken together, studies on BATF2 in various cancer types have shown that it generally inhibits tumour growth and metastasis.

This study broadens the perspective that genes upregulated in tumour tissues are not necessarily oncogenes [57, 58]. CXCL11 was highly expressed in tumour tissues; however, patients in the high-expression group had a longer survival time. We observed that higher expression levels of CXCL11 in tumour tissues were associated with an increased presence of CD8 T cells. This may be attributable to the gene's role in activating immune cells that exert anti-cancer effects [59]. The PLK1 gene is overexpressed in many tumour types, and PLK1 gene overexpression is often directly related to poor prognosis, whereas in breast cancer, PLK1 overexpression is associated with longer survival. PLK1 overexpression has tumour-suppressive properties by disrupting tumour cell mitosis and cytokinesis [60]. Gene expression and function may be affected by the stage of tumour development, changes in the microenvironment, and the mode of treatment [61–63]. In the early stages of tumours, these genes may have anti-cancer functions, such as inhibiting tumour growth or promoting apoptosis. In advanced tumours, mutations, treatment pressures, or other factors may alter the function of these genes, leading them to promote tumour growth and spread. This dynamic makes cancer research and treatment extremely complex. Understanding the mechanisms of these changes is critical for developing effective treatment strategies, and future research needs to further uncover the specific mechanisms of these dynamic changes to better address these challenges.

5 Conclusions

BATF2 is closely related to PD-L1 expression in GC. High BATF2 expression positively correlates with low PD-L1 expression, tumour cell growth inhibition, and longer patient survival times. The evidence from the present in vitro studies implies that the candidate gene BATF2 shows promise for predicting the efficacy of PD-1/PD-L1 inhibitors in patients with GC. However, further preclinical testing of the effects of this candidate gene BATF2 on the clinical outcome and prognosis of immunotherapy in both immunocompetent or nude mouse models bearing mouse and human GC cells is needed.

Acknowledgements Not applicable

Author contributions All authors contributed to the study's conception and design. X.Z.D designed the study, and B.Y.L and H.L.L wrote the main manuscript text. F.E.Z and X.Y.L performed the data analysis. B.Q.L and Z.Z.W provided technical and material support. X.Z.D, L.Z, and B.Y.L revised the manuscript. All authors reviewed and approved the final version of the manuscript. B.Y.L and H.L.L contributed equally to this study.

Funding This work was supported by the National Natural Science Foundation of China (Nos. 82271765, 81773778), Talent Project established by the Chinese Pharmaceutical Association Hospital Pharmacy department (No.CPA-Z05-ZC-2023-003), Beijing Hospitals Authority Youth Programme (Code: QML20230811).

Data availability The datasets used and analysed in the present study are available from the public sources described. All data generated or analysed during this study are included in this published article (and its supplementary information files).

Declarations

Ethics approval and consent to participate The Ethics Committee of the Chinese People's Liberation Army General Hospital approved all animal procedures (Approval No. 2019-X15-85).

Consent to publications Not applicable.

Competing interests The authors declare no competing interests.

References

1. Wang G, et al. Immunotherapy and targeted therapy as first-line treatment for advanced gastric cancer. Crit Rev Oncol Hematol. 2024;198:104197.
2. Wang X, et al. Safety and efficacy of immunotherapy plus chemotherapy as neoadjuvant treatment for patients with locally advanced gastric cancer: a retrospective cohort study. Invest New Drugs. 2023;41(4):579–86.
3. An M, et al. Early immune remodeling steers clinical response to first-line chemoimmunotherapy in advanced gastric cancer. Cancer Discov. 2024;14(5):766–85.
4. Christodoulidis G, Koumarelas KE, Kouliou MN. Revolutionizing gastric cancer treatment: the potential of immunotherapy. World J Gastroenterol. 2024;30(4):286–9.
5. Mou P, et al. Research progress on the immune microenvironment and immunotherapy in gastric cancer. Front Immunol. 2023;14:1291117.
6. Pabst L, et al. Prognostic and predictive biomarkers in the era of immunotherapy for lung cancer. Int J Mol Sci. 2023;24(8):7577.
7. Holder AM, et al. Defining clinically useful biomarkers of immune checkpoint inhibitors in solid tumours. Nat Rev Cancer. 2024;24:498–512.
8. Topalian SL, et al. Mechanism-driven biomarkers to guide immune checkpoint blockade in cancer therapy. Nat Rev Cancer. 2016;16(5):275–87.
9. Fuchs CS, et al. Safety and efficacy of pembrolizumab monotherapy in patients with previously treated advanced gastric and gastroesophageal junction cancer: phase 2 clinical KEYNOTE-059 Trial. JAMA Oncol. 2018;4(5):e180013.
10. Feng XS, et al. Prognostic significance of PD-L1 expression in patients with gastric cancer in East Asia: a meta-analysis. Onco Targets Ther. 2016;9:2649.
11. Patel SP, Kurzrock R. PD-L1 expression as a predictive biomarker in cancer immunotherapy. Mol Cancer Ther. 2015;14(4):847–56.
12. Rittmeyer A, et al. Atezolizumab versus docetaxel in patients with previously treated non-small-cell lung cancer (OAK): a phase 3, open-label, multicentre randomised controlled trial. Lancet. 2017;389(10066):255–65.
13. Yu-Fei LI, et al. Expression of PD1/PD-L1 in gastric carcinoma and its correlation with clinicopathological characteristics and prognosis. Chin J Clin Exp Pathol. 2018;34(06):614–8.
14. Zhao JJ, et al. Low programmed death-ligand 1-expressing subgroup outcomes of first-line immune checkpoint inhibitors in gastric or esophageal adenocarcinoma. J Clin Oncol. 2022;40(4):392–402.
15. Lu Z, et al. The combination of gene hyperamplification and PD-L1 expression as a biomarker for the clinical benefit of tislelizumab in gastric/gastroesophageal junction adenocarcinoma. Gastric Cancer. 2022;25(5):943–55.
16. Sharma P, et al. The next decade of immune checkpoint therapy. Cancer Discov. 2021;11(4):838–57.
17. Szklarczyk D, et al. STRING v11: protein-protein association networks with increased coverage, supporting functional discovery in genome-wide experimental datasets. Nucleic Acids Res. 2019;47(D1):D607-d613.
18. Ucaryilmaz Metin C, Ozcan G. Comprehensive bioinformatic analysis reveals a cancer-associated fibroblast gene signature as a poor prognostic factor and potential therapeutic target in gastric cancer. BMC Cancer. 2022;22(1):692.
19. Zhang P, et al. Dissecting the single-cell transcriptome network underlying gastric premalignant lesions and early gastric cancer. Cell Rep. 2019;27(6):1934-1947.e5.
20. Xie JW, et al. m(6)A modification-mediated BATF2 acts as a tumor suppressor in gastric cancer through inhibition of ERK signaling. Mol Cancer. 2020;19(1):114.
21. Henley MJ, Koehler AN. Advances in targeting "undruggable" transcription factors with small molecules. Nat Rev Drug Discov. 2021;20(9):669–88.
22. Yoon YH, et al. Upregulation of complement factor H by SOCS-1/3¯STAT4 in lung cancer. Cancers (Basel). 2019;11(4):471.
23. Kang YK, et al. Nivolumab in patients with advanced gastric or gastro-oesophageal junction cancer refractory to, or intolerant of, at least two previous chemotherapy regimens (ONO-4538-12, ATTRACTION-2): a randomised, double-blind, placebo-controlled, phase 3 trial. Lancet. 2017;390(10111):2461–71.
24. Janjigian YY, et al. First-line nivolumab plus chemotherapy versus chemotherapy alone for advanced gastric, gastro-oesophageal junction, and oesophageal adenocarcinoma (CheckMate 649): a randomised, open-label, phase 3 trial. The Lancet. 2021;398(10294):27–40.

25. Topalian SL, et al. Survival, durable tumor remission, and long-term safety in patients with advanced melanoma receiving nivolumab. J Clin Oncol. 2014;32(10):1020–30.
26. Rizvi NA, et al. Activity and safety of nivolumab, an anti-PD-1 immune checkpoint inhibitor, for patients with advanced, refractory squamous non-small-cell lung cancer (CheckMate 063): a phase 2, single-arm trial. Lancet Oncol. 2015;16(3):257–65.
27. Ansell SM, et al. PD-1 Blockade with nivolumab in relapsed or refractory Hodgkin's lymphoma. N Engl J Med. 2015;372(4):311–9.
28. Wainberg ZA, et al. Efficacy of pembrolizumab monotherapy for advanced gastric/gastroesophageal junction cancer with programmed death ligand 1 combined positive score ≥10. Clin Cancer Res. 2021;27(7):1923–31.
29. Tabernero J, et al. KEYNOTE-859: a Phase III study of pembrolizumab plus chemotherapy in gastric/gastroesophageal junction adenocarcinoma. Future Oncol. 2021;17(22):2847–55.
30. Bellmunt J, et al. Pembrolizumab as second-line therapy for advanced urothelial carcinoma. N Engl J Med. 2017;376(11):1015–26.
31. Armand P, et al. Five-year follow-up of KEYNOTE-087: pembrolizumab monotherapy for relapsed/refractory classical Hodgkin lymphoma. Blood. 2023;142(10):878–86.
32. Schmid P, et al. Pembrolizumab for early triple-negative breast cancer. N Engl J Med. 2020;382(9):810–21.
33. Nishikawa H, Sakaguchi S. Regulatory T cells in cancer immunotherapy. Curr Opin Immunol. 2014;27:1–7.
34. Haist M, et al. The functional crosstalk between myeloid-derived suppressor cells and regulatory T cells within the immunosuppressive tumor microenvironment. Cancers (Basel). 2021;13(2):210.
35. Oweida A, et al. Resistance to radiotherapy and PD-L1 blockade is mediated by TIM-3 upregulation and regulatory T-cell infiltration. Clin Cancer Res. 2018;24(21):5368–80.
36. Roland CL, et al. Cytokine levels correlate with immune cell infiltration after anti-VEGF therapy in preclinical mouse models of breast cancer. PLoS ONE. 2009;4(11):e7669.
37. Wang DR, Wu XL, Sun YL. Therapeutic targets and biomarkers of tumor immunotherapy: response versus non-response. Signal Transduct Target Ther. 2022;7(1):331.
38. Formica V, et al. PD-L1 thresholds predict efficacy of immune checkpoint inhibition in first-line treatment of advanced gastroesophageal adenocarcinoma. A systematic review and meta-analysis of seven phase III randomized trials. ESMO Open. 2024;9(11):103967.
39. Yoon HH, et al. Association of PD-L1 expression and other variables with benefit from immune checkpoint inhibition in advanced gastroesophageal cancer: systematic review and meta-analysis of 17 phase 3 randomized clinical trials. JAMA Oncol. 2022;8(10):1456–65.
40. Shitara K, et al. Pembrolizumab versus paclitaxel for previously treated, advanced gastric or gastro-oesophageal junction cancer (KEYNOTE-061): a randomised, open-label, controlled, phase 3 trial. Lancet. 2018;392(10142):123–33.
41. Chen C, et al. Efficacy and safety of immune checkpoint inhibitors in advanced gastric or gastroesophageal junction cancer: a systematic review and meta-analysis. Oncoimmunology. 2019;8(5):e1581547.
42. Kim ST, et al. Comprehensive molecular characterization of clinical responses to PD-1 inhibition in metastatic gastric cancer. Nat Med. 2018;24(9):1449–58.
43. Samstein RM, et al. Tumor mutational load predicts survival after immunotherapy across multiple cancer types. Nat Genet. 2019;51(2):202–6.
44. Cornelison R, et al. Targeting AVIL, a new cytoskeleton regulator in glioblastoma. Int J Mol Sci. 2021;22(24):13635.
45. Roberts AW, et al. Targeting BCL2 with Venetoclax in Relapsed Chronic Lymphocytic Leukemia. N Engl J Med. 2016;374(4):311–22.
46. Han T, et al. The tumor-suppressive role of BATF2 in esophageal squamous cell carcinoma. Oncol Rep. 2015;34(3):1353–60.
47. Lin Y, et al. Expression and clinical implications of basic leucine zipper ATF-like transcription factor 2 in breast cancer. BMC Cancer. 2021;21(1):1062.
48. Li Y, et al. Exosomal miR-361-3p promotes the viability of breast cancer cells by targeting ETV7 and BATF2 to upregulate the PAI-1/ERK pathway. J Transl Med. 2024;22(1):112.
49. Zhou J, et al. Nuclear export of BATF2 enhances colorectal cancer proliferation through binding to CRM1. Clin Transl Med. 2023;13(5):e1260.
50. Kanemaru H, et al. Antitumor effect of Batf2 through IL-12 p40 up-regulation in tumor-associated macrophages. Proc Natl Acad Sci U S A. 2017;114(35):E7331-e7340.
51. Jiang Q, et al. CD36-BATF2\MYB axis predicts anti-PD-1 immunotherapy response in gastric cancer. Int J Biol Sci. 2023;19(14):4476–92.
52. Liu J, et al. BATF2 inhibits PD-L1 expression and regulates CD8+ T-cell infiltration in non-small cell lung cancer. J Biol Chem. 2023;299(11):105302.
53. Zhang X, et al. BATF2 prevents glioblastoma multiforme progression by inhibiting recruitment of myeloid-derived suppressor cells. Oncogene. 2021;40(8):1516–30.
54. Wen H, et al. Decreased expression of BATF2 is significantly associated with poor prognosis in oral tongue squamous cell carcinoma. Oncol Rep. 2014;31(1):169–74.
55. Ma H, et al. Decreased expression of BATF2 is associated with a poor prognosis in hepatocellular carcinoma. Int J Cancer. 2011;128(4):771–7.
56. Liu Z, Yang Y, Zhou X. BATF2 in human colorectal cancer. Aging (Albany, NY). 2015;7(5):284–5.
57. Moya IM, et al. Peritumoral activation of the Hippo pathway effectors YAP and TAZ suppresses liver cancer in mice. Science. 2019;366(6468):1029–34.
58. Wei WY, et al. E2F–1 overexpression inhibits human gastric cancer MGC-803 cell growth in vivo. World J Gastroenterol. 2015;21(2):491–501.
59. Cao Y, et al. CXCL11 Correlates with antitumor immunity and an improved prognosis in colon cancer. Front Cell Dev Biol. 2021;9:646252.
60. de Cárcer G, et al. Plk1 overexpression induces chromosomal instability and suppresses tumor development. Nat Commun. 2018;9(1):3012.
61. Colantuoni C, et al. Temporal dynamics and genetic control of transcription in the human prefrontal cortex. Nature. 2011;478(7370):519–23.
62. Shalek AK, et al. Single-cell RNA-seq reveals dynamic paracrine control of cellular variation. Nature. 2014;510(7505):363–9.
63. de Visser KE, Joyce JA. The evolving tumor microenvironment: from cancer initiation to metastatic outgrowth. Cancer Cell. 2023;41(3):374–403.